Notch3 drives development and progression of cholangiocarcinoma

Rachel V. Guest[a,b,1], Luke Boulter[a,c], Benjamin J. Dwyer[a], Timothy J. Kendall[c,d], Tak-Yung Man[a], Sarah E. Minnis-Lyons[a], Wei-Yu Lu[a], Andrew J. Robson[b,d], Sofia Ferreira Gonzalez[a], Alexander Raven[a], Davina Wojtacha[a], Jennifer P. Morton[e], Mina Komuta[f], Tania Roskams[f], Stephen J. Wigmore[b,d], Owen J. Sansom[e], and Stuart J. Forbes[a,g,1]

[a]Medical Research Council Centre for Regenerative Medicine, University of Edinburgh, Edinburgh EH16 4UU, United Kingdom; [b]Department of Surgery, Royal Infirmary of Edinburgh, Edinburgh EH16 4SA, United Kingdom; [c]Medical Research Council Human Genetics Unit, Institute for Genetics and Molecular Medicine, University of Edinburgh, Edinburgh EH4 2XU, United Kingdom; [d]Medical Research Council Centre for Inflammation Research, Queens Medical Research Institute, University of Edinburgh, Edinburgh EH16 4TJ, United Kingdom; [e]Cancer Research UK Beatson Institute, Glasgow G61 1BD, United Kingdom; [f]Translational Cell & Tissue Research Unit, Katholieke Universiteit Leuven, 3000 Leuven, Belgium; and [g]The Scottish Liver Transplant Unit, Royal Infirmary of Edinburgh, Edinburgh EH16 4SA, United Kingdom

Edited by David Tuveson, Cold Spring Harbor Laboratory, Cold Spring Harbor, NY, and accepted by Editorial Board Member Elliott Kieff September 9, 2016 (received for review January 23, 2016)

The prognosis of cholangiocarcinoma (CC) is dismal. Notch has been identified as a potential driver; forced exogenous overexpression of Notch1 in hepatocytes results in the formation of biliary tumors. In human disease, however, it is unknown which components of the endogenously signaling pathway are required for tumorigenesis, how these orchestrate cancer, and how they can be targeted for therapy. Here we characterize Notch in human-resected CC, a toxin-driven model in rats, and a transgenic mouse model in which p53 deletion is targeted to biliary epithelia and CC induced using the hepatocarcinogen thioacetamide. We find that across species, the atypical receptor NOTCH3 is differentially overexpressed; it is progressively up-regulated with disease development and promotes tumor cell survival via activation of PI3k-Akt. We use genetic KO studies to show that tumor growth significantly attenuates after Notch3 deletion and demonstrate signaling occurs via a noncanonical pathway independent of the mediator of classical Notch, Recombinant Signal Binding Protein for Immunoglobulin Kappa J Region (RBPJ). These data present an opportunity in this aggressive cancer to selectively target Notch, bypassing toxicities known to be RBPJ dependent.

cholangiocarcinoma | Notch | noncanonical | bile duct | cancer

Cholangiocarcinoma (CC) is an aggressive primary liver malignancy with an increasing global incidence. Surgery remains the only potential cure, but few patients present with operable disease. New adjuvant treatments are urgently required; however, few targets have been put forward and none have been shown to have efficacy.

Notch is a master regulator of cell fate in the mammalian liver. In the embryo, hepatoblast specification to a biliary fate and tubulogenesis are dependent on Recombinant Signal Binding Protein for Immunoglobulin Kappa J Region (RBPJ)-driven effector transcription, i.e., canonical Notch signaling (1). Furthermore niche-derived ligand reactivates Notch during biliary injury in the adult to expand the hepatic progenitor cell (HPC) pool for repair (2). The four receptors play distinct roles, as evidenced by the spectrum of phenotypes seen after transgenic KO, as well in vitro and in vivo studies of HPC differentiation (3). Aberrant activation of Notch paralogs results in a spectrum of cancer phenotypes (4), implying differing potentials for therapeutic targeting. Their individual contribution to biliary carcinogenesis remains unclear.

A population of periportal hepatocytes has been identified enriched for biliary gene expression, with special replicative capacity and potential for parenchymal regeneration during hepatocyte injury (5). Introduction of transgenically activated, supraphysiological levels of Notch1 intracellular domain (N1-ICD) in hepatocytes can redirect cell identity to a ductular lineage, activating the cancer program (6, 7). There is further evidence that after damage, hepatocytes can contribute to the HPC pool, adopting biliary-specific functions, and that this reverses during recovery (8). This potential for hepatocyte plasticity may explain the appearance of perivenular CC in chronic hepatitis C virus (HCV) infection. We used lineage tracing to demonstrate CC can arise from $CK19^+$ ductular cells; however, the contribution from biliary vs. hepatocyte-derived HPCs and the CC cell of origin is still hotly debated.

Oncogenic Notch1 is a driver of a proportion of T-cell acute lymphoblastic leukemias, whereas other tumors rarely exhibit mutated Notch; rather, WT signaling is dysregulated. Sequencing of CC has failed to identify *NOTCH* mutations, and therefore we sought to evaluate the contribution of endogenous WT Notch. As the role of Notch in cancer depends on somatic context, we aimed to use a range of models to reflect the mutational heterogeneity of CC. Both pan-receptor and Notch1 inhibition are associated with off-target effects, so we hypothesized that characterizing the signal might identify specific drivers to enable targeting to bypass toxicity.

Significance

Clinical outcomes in cholangiocarcinoma (CC) are poor; few patients are candidates for curative resection, and palliative chemotherapy produces only modest effects on survival. With an increasing incidence, new targets are urgently needed. Notch has been identified as having potential to induce CC when transgenically overexpressed, and this study aimed to characterize how endogenous Notch might drive tumorigenesis. We identify the atypical receptor Notch3 as differentially overactivated in CCs in humans, rats, and mice, with genetic deletion significantly reducing CC growth. Notch3 sustains tumor cell survival through PI3k/Akt activation via a noncanonical mechanism independent of Recombinant Signal Binding Protein for Immunoglobulin Kappa J Region (RBPJ), presenting an opportunity to target the pathway without disrupting classical Notch and bypassing toxicities associated with γ-secretase inhibitors.

Author contributions: R.V.G., L.B., S.E.M.-L., A.J.R., J.P.M., T.R., S.J.W., O.J.S., and S.J.F. designed research; R.V.G., L.B., B.J.D., T.-Y.M., S.E.M.-L., W.-Y.L., A.J.R., S.F.G., A.R., D.W., and M.K. performed research; J.P.M. contributed new reagents/analytic tools; R.V.G., L.B., B.J.D., T.J.K., T.-Y.M., and W.-Y.L. analyzed data; and R.V.G., T.R., S.J.W., O.J.S., and S.J.F. wrote the paper.

The authors declare no conflict of interest.

This article is a PNAS Direct Submission. D.T. is a Guest Editor invited by the Editorial Board.

Freely available online through the PNAS open access option.

[1]To whom correspondence may be addressed. Email: rachel.guest@ed.ac.uk or stuart.forbes@ed.ac.uk.

This article contains supporting information online at www.pnas.org/lookup/suppl/doi:10.1073/pnas.1600067113/-/DCSupplemental.

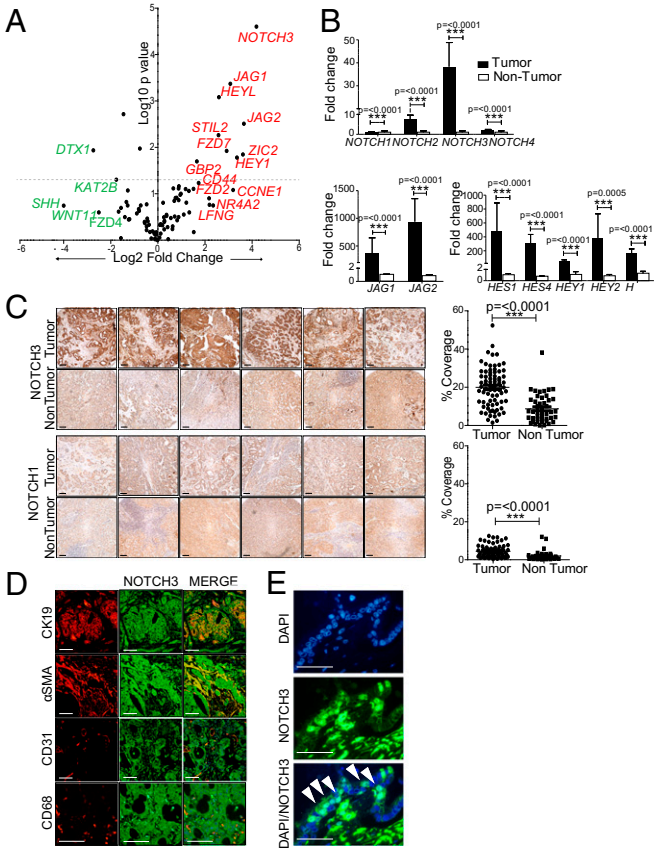

Fig. 1. Notch3 is differentially activated in human CC. (*A*) Volcano plot of rt-PCR Notch array in human CC and patient-matched liver ($n = 5$, $n = 5$). Gray line represents *P* value of 0.05. Red labels, up-regulation at least fourfold; green, down-regulation at least fourfold. (*B*) Notch expression in human CC ($n = 48$) and healthy liver ($n = 42$) (RT-PCR). Medians compared with Mann–Whitney *U* test. (*C*) Tissue microarray human CC ($n = 77$) and noncancerous liver ($n = 47$). Representative Notch1 and Notch3 immunostaining (positive and isotype controls; Fig. S1 *B* and *C*). Filled arrowheads, Notch3$^+$ ductules and vascular smooth muscle in healthy liver. Pixel analysis of CC and controls compared with Mann–Whitney *U* test. (*D*) Dual fluorescence of Notch3 (green) in human CC with αSMA, CD31$^+$, or CD68$^+$ (red) (Scale bar, 100 μm.) (*E*) N3-ICD (green) in human CC (white filled arrowheads). (Scale bar, 50 μm.) Data are means ± SEM. $^*P \le 0.05$, $^{**}P \le 0.01$, $^{***}P \le 0.001$.

Results

Notch3 Is Differentially Activated in Human CC. We used a targeted *NOTCH* PCR array in five surgically resected samples paired with matched noncancerous liver (Fig. 1*A* and Table S1; four perihilar and one mass-forming intrahepatic CC, all moderately differentiated adenocarcinoma). *NOTCH3* was highly up-regulated: 18.2-fold ($P \le 0.000025$); *NOTCH1*, 1.9-fold ($P = 0.105153$); *NOTCH2*, 1.8-fold ($P = 0.076917$), and *NOTCH4*, 1.6-fold ($P = 0.076371$). Up-regulation of *JAG1* (8.4-fold, $P = 0.000426$) and *JAG2* (12.6-fold, $P = 0.003088$) indicated that signaling may be triggered by nearby ligand. This preliminary screen suggested pathway activity, with up-regulation of the Hes/Hey family of effectors: *HEY1*, 10.25-fold, ($P = 0.016558$); and *HEYL*, 6.0-fold ($P = 0.000829$), although in this cohort, there was no change in the archetypal effector of classical Notch, *HES1* (0.9-fold, $P = 0.687197$; Fig. 1*A*). We expanded the analysis to a larger cohort of 48 CC cases and compared them with healthy livers using quantitative RT-PCR (qRT-PCR; $n = 42$). *NOTCH3* was again up-regulated 38-fold ($P \le 0.0001$), with *NOTCH1*, 1.1-fold ($P \le 0.0001$); *NOTCH2*, 7.5-fold ($P \le 0.0001$); *NOTCH4*, 2.0 fold ($P \le 0.0001$); *JAG1*, 363.3-fold ($P \le 0.0001$); *JAG2*, 938.6-fold ($P \le 0.0001$); *HES1*, 483.7-fold ($P \le 0.0001$); *HES4*, 304.2-fold ($P \le 0.0001$); *HEY1*, 46.8-fold ($P \le 0.0001$); *HEY2*, 384.4-fold ($P = 0.0005$), *HEYL*, 160.6-fold ($P \le 0.0001$) (Fig. 1*B*). We stained the cohort and a tissue CC microarray for Notch receptors with a panel of cell-specific markers. In the healthy liver, we observed little expression of NOTCH1 (Fig. 1*C* and Fig. S1 *A* and *B*) in contrast to NOTCH3, which was consistently seen on vascular smooth muscle (Fig. S1*A*) and on many, although not all, bile ducts (Fig. 1*C* and Fig. S1*A*). Large regions of almost all tumors stained positively for NOTCH3 (19 ± 0.77% displayed >10% coverage; 31 ± 0.84% displayed >20%; 1.6 ± 5.40% displayed >40%). Pixel analysis showed mean coverage of each core was 56.2% greater in tumors compared with noncancerous controls (Fig. 1*C*). NOTCH1 positivity was also greater in tumors, but not to the same extent (mean coverage, 4.49 ± 3.17% tumors vs. 2.03 ± 0.43% nontumors). In all CC samples, positivity colocalized with CK19, and a subset of tumors also exhibited stromal positivity, colocalizing with the myofibroblast marker α-SMA (Fig. 1*D* and Fig. S1*D*). NOTCH3 did not colocalize with endothelial or inflammatory cell markers (CD31 and CD68) (Fig. 1*D*). In malignant ductules, NOTCH3 was frequently nuclear; reactivity of the intracellular domain (N3-ICD) suggested functionality (Fig. 1*E*). To corroborate this, we performed N3-ICD immunoblotting: the mean signal of N3-ICD (normalized to β-actin) was 95 ± 74.66 times greater in tumor vs. matched nontumor lysates ($P = 0.0286$; Fig. S1*E*). Almost all tumors exhibited stromal expression of JAGGED1 (Fig. S1*F*).

Notch3 Is Differentially Up-Regulated During CC Development. To determine the contribution of Notch to CC development, we used a well-characterized toxin-induced model in rat using the hepatocarcinogen thioacetamide (TAA) to induce injury followed by cancer (9). After 16 wk, multifocal foci of the invasive CC are seen with mucin production and desmoplasia. The model has a penetrance of 100% at 20 wk, when tumors are numerous, large, and coalescent (Fig. S2*A*). We used a *Notch* PCR array to compare expression in uninjured animals to those with inflammation (8- to 10-wk TAA) (Fig. 2*A*, *Left*), fibrosis (12–14 wk), early malignancy (20 wk), and invasive adenocarcinoma (26 wk) (Fig. 2*A*, *Right*, and Table S2). An induction in transcription was observed in line with tumor development as confirmed with qPCR (Fig. 2*B*); *Notch3* was a highly up-regulated receptor at 26 wk (52.01-fold by qRT-PCR; $P = 0.0022$), contrasted by modest up-regulation of *Notch1* (5.32-fold, $P = 0.0411$), *Notch2* (4.75-fold, $P = 0.0022$), and *Notch4* (9.67-fold, $P = 0.0022$). *Jag1* was up-regulated 24.00-fold ($P = 0.0022$). We saw nonsignificant up-regulation of *Jag2* (2.35-fold, $P = 0.3095$), and unlike in human disease, no change in effector transcription: *Hes1*, 0.67-fold ($P = 0.3095$); *Hey1*, 0.70-fold ($P = 0.3095$); *Hey2*, 0.77-fold ($P = 0.3939$); and *HeyL*, 2.10-fold ($P = 00649$). Immunostaining the time course mirrored these data; up-regulation occurred in line with tumor expansion, with Jagged1 and Notch3 in stroma and malignant ducts (Fig. 2*C*).

Reports demonstrated an inhibitory effect using γ-secretase inhibitors (GSIs) in CC cell lines and xenograft models. We aimed to evaluate efficacy on in vivo CC growth in a model where desmoplastic CC arises from the liver without transgenic overactivation of Notch. We administered *N*-[*N*-(3,5-difluorophenacetyl)-L-alanyl]-*S*-phenylglycine *t*-butyl ester (DAPT) to rats on the TAA protocol, treating animals during the last 5 wk of injury, i.e., once tumors had established (Fig. S3*A*). TAA damage was equivalent in the two groups (Fig. S3*B*). Following DAPT, liver-to-body weight ratio was reduced by 19 ± 0.53% ($P = 0.0121$; Fig. S3*C*), and the proportion of liver infiltrated by the tumor was reduced by 78 ± 0.84% ($P = 0.0148$; Fig. 3*B*). There was no apparent difference in the microscopic appearance of DAPT-treated tumors; all cancerous foci exhibited features of well-differentiated adenocarcinoma with mucin production and desmoplasia, with no apparent difference in cell death or necrosis histologically. Moreover, tumor number was unchanged, consistent with the observation that by 21 wk, tumors are established

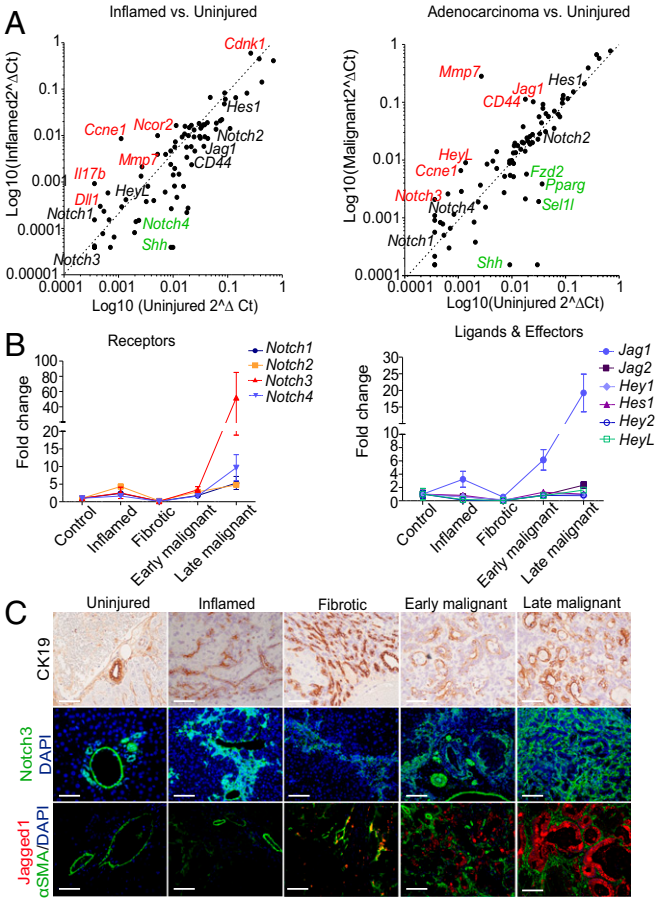

Fig. 2. Notch3 is differentially up-regulated during CC development. (*A*) PCR Notch pathway array in rats after 600 mg/L TAA for 8–10 wk (inflamed) ($n = 6$) vs. control (*Left*) and 24–26 wk (adenocarcinoma) ($n = 6$) vs. control ($n = 6$) (*Right*). Red labels, at least fourfold up-regulation; green, at leat fourfold down-regulation. (*B*) qRT-PCR of Notch expression in TAA rat liver normalized to uninjured controls at 8–10 (inflamed), 12–14 (fibrotic), 20 (early malignant), and 26 wk (late malignant) ($n = 3$; $n = 6$ control). (*C*) IHC of TAA time course. CK19 (DAB). Notch3, green; Jagged1, red; αSMA, green. (Scale bar, 100 μm.)

and DAPT after this point slows CC growth. To establish that inhibition of the γ-secretase complex resulted in a reduction in signaling via Notch3, we stained for the Notch3 protein and looked for nuclear positivity, i.e., Notch3 intracellular domain (Fig. S3*D*). Immunostaining for the proliferation marker Ki67 demonstrated a 38.15% reduction in cycling cells in tumor cells ($P = 0.0005$; 244.14 ± 10.03 vehicle vs. 150.99 ± 20.40 DAPT; Fig. 3*D*).

Genetic Deletion of Notch3 Reduces CC Formation and Progression. γ-Secretase is a large protease complex, and, although blockade results in total loss of Notch signal (single point mutation causes embryonic lethality) (10), Notch is only one of its substrates. Notch3 is an atypical receptor with structural differences to Notch1 and 2 and can be targeted without disrupting normal development (11). We therefore aimed to evaluate its potential as a nonredundant CC driver using genetic Notch3 deletion. Loss of the tumor suppressor p53 is a common occurrence in CC (12). CC arises following chronic inflammation as in primary sclerosing cholangitis. We therefore used a mouse model in which loss of *Tp53* is conditionally targeted to enhanced yellow fluorescent protein (eYFP)-labeled CK19$^+$ epithelia using tamoxifen inducible Cre recombinase (CK19CreER^{T}eYFPp53$^{f/f}$) followed by injury with TAA to induce oncogenic stress (13). At 26 wk, multifocal invasive CC was observed in livers of CK19CreYFPp53$^{f/f}$ mice at 80% penetrance, but not CK19CreYFPp53$^{wt/f}$ or CK19CreYFPp53$^{wt/wt}$ mice (Fig. S4*A*). Tumors stained for ductular markers CK19 and Sox9, and these frequently but not exclusively colocalized with eYFP (Fig. 4*A*), in line with the weak efficiency of Cre recombination in this model (14). In tumors, eYFP$^+$ epithelia were almost always positive for NOTCH3, although not all NOTCH3$^+$ cells carried the heritable eYFP label, indicating p53 loss is not required for Notch3 induction. In mice, we observed apparently less stromal Notch3 positivity (Fig. 4*A*, *Bottom*).

Notch3 mRNA and to a lesser degree *Notch2*, but not *Notch1* or *Notch4* (undetectable), was overexpressed in CC in CK19CreYFPp53$^{f/f}$ mice compared with CK19CreYFPp53$^{wt/f}$ and CK19CreYFPp53$^{wt/wt}$ mice, as well as CK19CreYFPp53$^{f/f}$ mice without CC (Fig. 4*B*). When normalized to CK19CreYFPp53$^{wt/wt}$ mice with 26 wk of TAA, *Notch3* is up-regulated 85.92-fold ($P = 0.0286$) in CK19CreYFPp53$^{f/f}$ mice with CC, compared with *Notch1* at 24.28-fold ($P = 0.0286$). In CK19CreYFPp53$^{f/f}$ mice that did not develop CC, *Notch3* was up-regulated 41.35-fold ($P = 0.0286$), compared with *Notch1* at 14.94-fold ($P = 0.0381$). Nonsignificant increases in *Jag1* and *Jag2* were observed and the only effector to reach significance was *Hey2*: 45.47-fold ($P = 0.0286$; Fig. 4*B*).

We then compared tumor burden in CK19CreER^{T}eYFPp53$^{f/f}$ mice on the TAA protocol to mice carrying constitutive deletion of the *Notch3* gene (CK19CreER^{T}p53$^{f/f}$N3). A difference in livers in N3$^{+/+}$ mice compared with N3$^{+/-}$ and N3$^{-/-}$ animals was seen at 26 wk (Fig. 5*A*). Although macroscopic cancerous nodules were not numerous on the liver surface of mice of any genotype, microscopic foci of invasive CC were clearly evident in all groups (Fig. 5 *A* and *C*). A 99.14 ± 0.48% reduction was seen in liver infiltrated by tumor in N3$^{+/-}$ mice, as well as a reduction in the mean tumor number [28.78 ± 15.37 N3$^{+/+}$ mice ($n = 9$) vs. 0.875 ± 0.38 N3$^{+/-}$ mice ($n = 8$)], indicating single copy loss of *Notch3* is sufficient to inhibit CC formation (Fig. 5*B* and Fig. S5*A*). N3$^{-/-}$ mice exhibited a similar phenotype; there was no statistical difference in tumor burden to N3$^{+/-}$ animals (N3$^{+/-}$ mice, 0.035 ± 0.01 mean% tumor area vs. 0.086 ± 0.05 N3$^{-/-}$). Staining for pan-cytokeratin and pERK demonstrated an apparent reduction in proliferating malignant ductules in mice with Notch3 deletion (Fig. 5*C*). No significant compensatory up-regulation of *Notch1, Notch2*, or *Notch4* was observed in

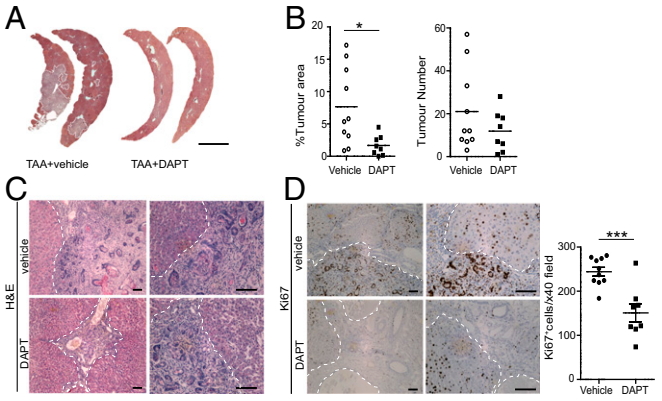

Fig. 3. Pan-inhibition of Notch reduces CC progression. (*A*) Tiled low power photomicrographs of rat liver after TAA with DAPT or vehicle during weeks 21–26. (Scale bar, 100 mm.) (*B*) (*Left*) Proportion of liver infiltrated by CC after DAPT ($n = 8$) vs. vehicle ($n = 10$) ($P = 0.0148$). (*Right*) Tumor number in rats treated with DAPT or vehicle ($P = 0.2856$). Data are means ± SEM. Medians compared with Mann–Whitney *U* test (*$P \leq 0.05$). (*C*) High- and low-power H&E sections of rat liver after vehicle (*Upper*) or TAA (*Lower*). Dashed lines are tumor boundary. (*D*) Ki67 immunostaining and quantification of rat liver sections after vehicle or TAA. (Scale bar, 100 μm.) Number of Ki67-positive tumor cells per ×40 field (30 fields per rat) compared using Student *t* test. *$P \leq 0.05$, **$P \leq 0.01$, ***$P \leq 0.001$.

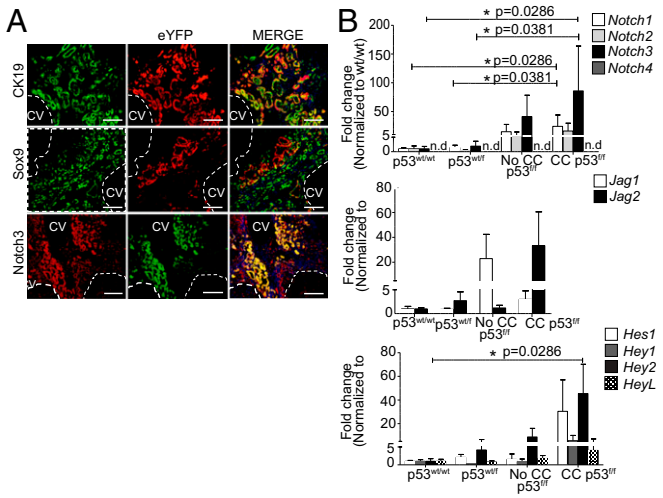

Fig. 4. Notch3 is overexpressed in a transgenic mouse model of CC. (*A*) Cofluorescence of CK19 (green) and eYFP (red) (*Top*); Sox9 (green) and eYFP (red) (*Middle*), and Notch3 (red) with eYFP (green) (*Bottom*) in CC foci from CK19CreER^{T}R26ReYFPp53$^{f/f}$ mice after 26-wk TAA (CV, central vein; dashed line tumor boundary) (Scale bar, 100 μm.) (*B*) qRT-PCR of whole liver from CK19CreYFPp53$^{f/f}$ mice after 26-wk TAA. Comparisons between single groups are represented on a single graph for clarity; however, individual Mann–Whitney *U* tests used to compare individual genes between genotypes (p53$^{wt/wt}$, $n = 4$; p53$^{wt/f}$, $n = 6$; p53$^{f/f}$ no CC, $n = 3$; p53$^{f/f}$ with CC, $n = 4$) Data are means ± SEM.

response to *Notch3* deletion (Fig. S5*B*). To evaluate the role of Notch1 in CC development, CK19CreER^{T}eYFPp53$^{f/f}$N1$^{f/f}$ mice were induced with tamoxifen and given TAA. These animals did not tolerate injury; they exhibited weight loss and signs of hepatic failure (jaundice and ascites), suggesting a failure of liver regeneration (Fig. S5*C*).

To assess whether this role for Notch3 was reproducible in a human system, we stably inhibited the gene using shRNA in cultured human CC cells and xenografts. Immunofluorescence of receptors was performed on three lines, and one was selected (CC-LP-1) (Fig. S5*D*). Cells were transfected with four independent shRNA with puromycin resistance cassettes for stable selection or scrambled sequences for comparison (15). Across multiple colonies, transfection inhibited *NOTCH3* expression (Fig. S5 *E* and *F*). Almost total ablation of effectors was observed, suggesting functional signaling inhibition (Fig. S5*G*). Clone 1 exhibited efficient knockdown and was used for further experiments. In vitro, a modest attenuation in proliferation was observed [19.42 ± 2.87% reduction in 3-(4,5-dimethylthiazol-2-yl)-diphenyltetrazolium bromide (MTT) absorbance; $P = 0.0765$; Fig. S5*H*], and when xenografted, a 62 ± 28.74% reduction in size ($P = 0.0237$) and 76 ± 28.44% reduction in mass ($P = 0.0237$) was seen in Notch3 KD xenografts (Fig. 5*D*). We confirmed this was not due to reduced neoangiogenesis by quantification of CD31 (mean signal CD31 to DAPI, 0.0506 ± 0.0056 scrambled vs. 0.0285 ± 0.0079 N3shRNA xenografts; $P = 0.329$; Fig. S5*I*).

Genetic Silencing of Notch3 but Not RBPJ Reduces Signaling Through the PI3k-AKT Cascade. We then sought to identify potential targets preferentially activated by Notch3 that might drive cell survival or proliferation. To compare the immediate effects of knockdown on downstream signaling, we transfected human CC cells (CC-LP-1) with siRNA against either *NOTCH3* or the canonical effector *RBPJ*. Inhibition was confirmed with qRT-PCR and immunoblotting (Fig. S6 *A* and *B*). Eighty-four known drivers of hepatic carcinogenesis were screened with a PCR array (Tables S3 and S4). Almost all genes exhibiting changes in transcription (defined as at least fourfold) were either upstream mediators or downstream targets of the AKT cascade including *MET*, *IRS1*, and *XIAP* and the death receptors *FAS* and *FADD*. Surprisingly no changes were observed in response to RBPJ inhibition (Fig. 6*A* and Tables S3 and S4).

We therefore returned to previous models to assess whether induction of AKT by Notch3 held true in these systems. In shRNA Notch3 KD CC xenografts, pixel analysis revealed reduced phosphorylated AKT(Thr308) (0.537 ± 0.078 rodamine: DAPI signal scrambled vs. 0.346 ± 0.115 N3shRNA tumors), as well as phosphorylated downstream targets p-mTor (1.465 ± 0.675 scrambled vs. 0.606 ± 0.211 N3 shRNA) and pS6 (1.194 ± 0.322 scrambled vs. 0.379 ± 0.996 N3 shRNA; Fig. 6*B*). At the gene level, qPCR results mirrored the reduced transcription of targets identified in the siRNA-treated cells using the PCR array: *MET*, *IRS1*, *FAS*, and *RAC1* (Fig. S6*C*).

To confirm this phenomenon was not an off-target effect of RNAi, we looked at Akt in CK19CreER^{T}eYFPp53$^{f/f}$ mice on the TAA protocol with ($n = 8$) and without ($n = 9$) Notch3 deletion. A reduction in *Fas, Fadd*, and *Rac1* gene expression was seen, although this did not reach significance (Fig. S7*A*). Immunoblots, however, revealed a 72% reduction in pAKT protein (N3$^{+/-}$ 0.41 ± 0.10 vs. N3$^{-/-}$ 0.12 ± 0.06; $P = 0.0426$), a 30% reduction in pmTor (N3$^{+/-}$ 1.55 ± 0.13 vs. N3$^{-/-}$ 1.08 ± 0.13; $P = 0.0426$), a 54% reduction in pS6 (N3$^{+/-}$ 1.19 ± 0.13 vs. N3$^{-/-}$ 0.54 ± 0.16; $P = 0.0127$) and an 88% reduction in p70-S6 (N3$^{+/-}$ 0.91 ± 0.34 vs. N3$^{-/-}$ 0.11 ± 0.06; $P = 0.0593$; Fig. 7*A*). Finally, to independently verify Akt blockade reduces CC growth, we xenografted nude mice with WT CC cells, allowed tumors to establish, and systemically treated them with a small molecule inhibitor of PI3K, PI-103. At 28 d, we observed a 60.87% reduction in tumor size (mean volume, 228.07 ± 48.68 vs. 89.25 ± 32.54 mm^3 vehicle; $P = 0.0288$; Fig. S7*B*).

Discussion

Exogenous oncogene activation in mice can initiate carcinogenesis in many tissues and indeed often in tissues where these oncogenes

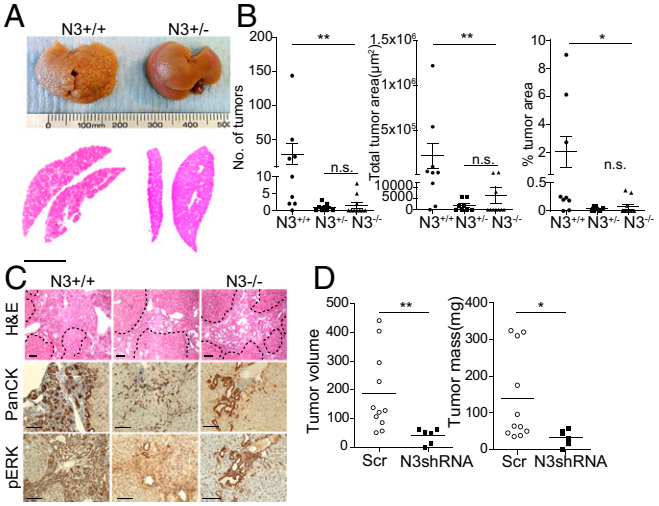

Fig. 5. Genetic deletion of Notch3 reduces CC formation and progression. (*A*) Photographs and tiled low-power photomicrographs of livers from CK19CreYFPp53$^{f/f}$N3$^{+/+}$ ($n = 9$) and CK19CreYFPp53$^{f/f}$N3$^{+/-}$ mice ($n = 8$) after 26-wk TAA. (Scale bar, 100 mm.) (*B*) Tumor number and total and % infiltrated liver area in N3$^{+/+}$, N3$^{+/-}$, and N3$^{-/-}$ mice after 26-wk TAA. Comparisons made with one-way ANOVA and Dunn's multiple comparison test for post hoc analyses. (*C*) Representative H&E-, pan-CK–, and pERK-stained sections from N3$^{+/+}$, N3$^{+/-}$, and N3$^{-/-}$ mice after 26-wk TAA. Dashed line, tumor boundary. (Scale bar, 100 μm.) (*D*) Tumor mass and volume of *NOTCH3* shRNA xenografts ($n = 6$) vs. scrambled control ($n = 11$). *$P \leq 0.05$, **$P \leq 0.01$, ***$P \leq 0.001$.

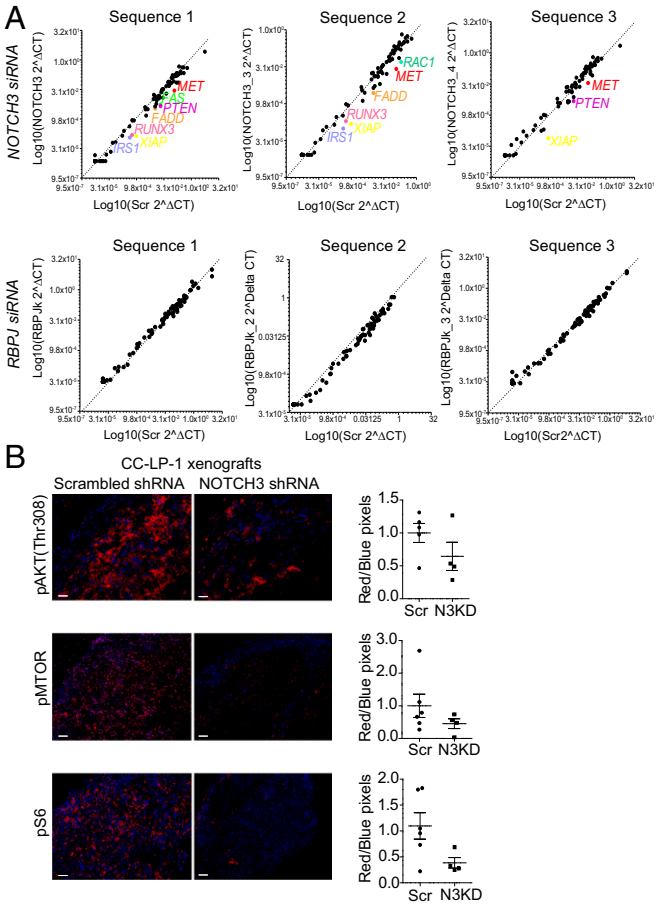

Fig. 6. Genetic silencing of Notch3, but not RBPJ, reduces PI3k-AKT transcription. (*A*) Human (CC-LP-1) cells transfected with *NOTCH3* or *RBPJ* siRNA and analyzed with oncogene PCR array. Three independent siRNA sequences were used, and RNA was pooled from three replicate wells for each sequence. Gene expression measured 48 h after transfection and compared with scrambled controls (dotted line represents no change in transcription). Genes in color are at least fourfold down-regulated. (*B*) IHC of pAKT(Thr308), pmTor, and pS6 with pixel analysis in Notch3 shRNA/scrambled CC-LP-1 xenografts. (Scale bar, 100 μm.)

are not overexpressed or mutated in human cancer. Consistent with the role of Notch as a cell fate determinant, transgenic overactivation of Notch1 (N1-ICD) in albumin-expressing cells results in biliary tumor formation (6, 7). In an almost identical model, however, N1-ICD expression under albumin and α-fetoprotein promoters produce HCC at 100% penetrance (16). Studies of KRAS and MYC show precise expression levels are critical to biological outcome. Because genomic analyses of CC conclude transforming Notch mutations are infrequent (17) and antibodies blocking Notch1 increase the number and extent of tumors (18), we aimed to elucidate the contribution of endogenous WT Notch to CC and identify components with potential for targeting.

We used CC models in three species not reliant on any one oncogenic alteration, and Notch3 is consistently overexpressed. As reported by others, Notch1 is barely detectable in the healthy adult liver (19). Conversely, Notch3 is consistently present around the vasculature, making the up-regulation observed in tumors all of the more striking. Notch3 up-regulation occurs with disease; the greatest increase occurs late during expansion and invasion. Overexpression is associated with functional activity as evidenced by consistent nuclear visualization of the intracellular domain. Inhibition in xenografted cells with shRNA or genetic KO in mice both result in attenuated tumor growth. This target, with many functions and interactions distinct from canonical signaling, offers an attractive prospect for therapy. Past work suggests antibody-mediated Notch3 inhibition has no effect on liver cancer; however, evidence of Notch3 activity in the model and antibody efficacy was lacking (18). In contrast, other work acknowledges that, in addition to Notch1, Notch3 is strongly expressed in human CC compared with the liver (7).

Notch3 drives 40% of non–small-cell lung cancers (NSCLCs) and almost all T-cell acute lymphoblastic leukemia. Tumor-inhibiting effects of GSIs are lost after Notch3 silencing in NSCLCs, suggesting cell survival is mediated via Notch3 (20). Serial transplantation studies indicate Notch3 is a regulator of self-renewal in tumor-propagating cells, and with no essential function in development or homeostasis (Notch3-null mice have no liver phenotype), Notch3 inhibition appears a safe strategy (11). GSIs have been pursued as therapy in a range of cancers, but translation has been hampered by toxicity. Such effects arise not due to disrupting the GS complex; the same phenotype occurs in RBPJ- or Hes1-deficient mice (21). Therefore, the possibility of a tumor-forming role via an RBPJ-independent mechanism is appealing. Our data suggest activation of AKT by Notch3 might be one such route.

Using independent techniques of blockade, we identify the PI3K/AKT pathway as one route of Notch3-driven cell survival; these data in line with Fan et al. who showed enhanced biliary tumorigenesis with transgenic activation of Notch and AKT (6). Many studies show the PI3K/AKT/mTor axis is dysregulated in CC, with AKT phosphorylation correlating with poor survival, and dual treatment with AKT and mTor inhibitors synergistically slowing tumor growth (22).

Although N-ICD translocation via RBPJ to drive Hes/Hey transcription is the most studied pathway, alternative modes of signaling are described including GS activation independent of ligand; N-ICD activity independent of RBPJ; or activation by membrane-tethered receptors without GS cleavage (23). RBPJ-independent signaling is characterized in T cells where N3-ICD interacts with IKKα to stimulate NF-κB and drive leukemia (24). Indeed, noncanonical Notch signaling is not uncommonly described in cancer, triggering cascades including PI3K/AKT, Wnt, and HIF1-α (25). Our data in rats of profound receptor overexpression without concomitant effector up-regulation further suggest Notch-driven CC can arise via an RBPJ-independent route, given the restriction of tumor growth after GSI.

The stimuli for Notch3 up-regulation are as yet unknown. In our rat time course, early ligand up-regulation by fibroblasts tempts speculation that stroma-derived factors might be a trigger. However, as tumors evolve, Jagged1 appears on ductules, suggesting a switch to autonomous signaling or activation of an alternative pathway. In ovarian carcinoma where Notch3 gene amplification is common, Jagged1 is itself dependent on Notch3 activity; deletion and ectopic

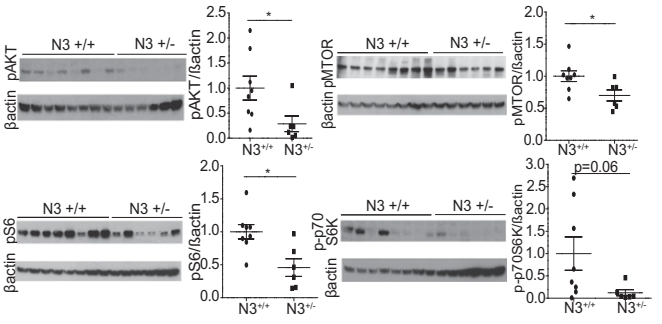

Fig. 7. Genetic silencing of Notch3 reduces activity through the PI3k-AKT cascade. Immunoblots and corresponding densitometry for p-Akt, p-mTor, p-S6, and p-p70 S6k from CK19CreYFPp53$^{f/f}$N3$^{+/+}$ and CK19CreYFPp53$^{f/f}$N3$^{+/-}$ livers after TAA. *$P \leq 0.05$.

expression inhibit and promote Jagged1, respectively, implementing a self-sustaining signaling loop (26). This role for Jagged1 is an important question as ligands are attractive alternative therapeutic targets. In *Drosophila, cis* interactions (receptor stimulated by ligand from the same cell) inhibit receptor activity within the cell while stimulating activity in neighboring cells. Potential for Jagged1 to exert differential effects on Notch1 and Notch3 here is intriguing.

Stimulation of the ductular response by Notch1 in biliary regeneration requires classical signaling via Hes1. Further work is needed to understand whether this signal required in CC, how it is affected by Notch3, if at all (we see no change in Notch1 following Notch3 inhibition), and how Hes/Hey are involved. Our data suggest this role is complex: we observe Hes/Hey up-regulation in human disease and mice but to a much lesser extent in rats. The fact we observe reduced Hes/Hey expression with Notch3 silencing and yet the observed changes in Akt-related components do not occur with RBPJ inhibition suggests that at least two signaling routes are active downstream of the receptor, and further mechanistic work is needed to understand this better. Taken together, however, our data suggest Notch3 is an important driver in CC and drives cell survival independently of RBPJ, opening up new therapeutic targets for this largely untreatable cancer.

Materials and Methods

Human Tissue. Human CC and liver were collected prospectively from patients undergoing resection at the Royal Infirmary Edinburgh with informed consent. The study was reviewed and approved by the Tayside Committee in Medical Research Ethics B. Retrospectively collected specimens were obtained from the National Health Service Lothian Scottish Academic Health Sciences Collaboration BioResource and healthy liver from the Edinburgh Medical Research Council Sudden Death Tissue bank. Tissue CC microarrays were purchased from Pantomics.

Animal Models and Xenografts. CK19CreER^{T}R26ReYFP mice (14) were a kind gift from Guoquaing Gu (Vanderbilt Medical Center, Nashville, TN). These mice were cross-bred with Trp53$_{tm1Brn}$ mice (p53$^{flox/flox}$) (ref. B6.129P2-Trp53tm1Brn/J), Notch3tm1Grid (N3$^{-/-}$) mice (ref. B6.129S1-Notch3^{tm1Grid}/J) (11), or or Notch1$^{fl/fl}$ (Notch1tmRko/Grid) from Jackson Laboratories. Trp53$_{tm1Brn}$ (p53$^{fl/fl}$) and Notch3tm1Grid (N3$^{-/-}$) mice were on a C57BL/6;C129 background; Notch1$^{fl/fl}$ mice were on a 129 background. Before experimental use, animals were cross-bred with the CK19CreER^{T}R26ReYFP line, which carried a CD1;C57BL/6 background. Progeny were subsequently on a mixed background and used for experimental comparison. In studies where Notch3 is altered, all experimental mice were from the same colony and had a consistent mixed background (CD1/C57BL/6/129). Throughout, littermates were included as controls where possible. All animals used were male and aged matched. Mice were genotyped by Transnetyx. LoxP recombination was induced with three doses of 4 mg tamoxifen (Sigma) in corn oil i.p. on alternate days at 6 wk of age. CC was induced using oral sweetened TAA (Sigma; 600 mg/mL) or vehicle for 26 wk (n = 8). Eight-week-old male Sprague–Dawley rats were given 600 mg/L sweetened oral TAA or vehicle for 26 wk (9). Animals were killed at 10, 12, 14, 16, 18, 20, 22, 24, and 26 wk (n = 3). Rats received 10 mg/kg DAPT (Tocris) in olive oil s.c. (n = 8) or olive oil alone (n = 12) thrice weekly during weeks 21–26.

Xenografts were performed on 6-wk-old CD1-nude mice with bilateral s.c. flank injection of the commercial CC line CC-LP-1 (5×10^5) (15) or CC-LP-1 cells transfected and stably selected for *NOTCH3* targeted shRNA or scrambled sequence control. Tumors were allowed to engraft for 28 d before mice were either killed or exposed to one of the following treatment regimes: DAPT (10 mg/kg), PI-103 (30 mg/kg, Selleckchem), or equivalent dose of vehicle for 14 d (n > 5 per group). Tumor volume was calculated using the modified ellipsoid formula: $0.5(l \times w^2)$. Animal studies were conducted in accordance with UK Home Office regulations under procedural guidelines, severity protocols, and with approval from the Animal Welfare and Ethical Approval Review Body (AWERB).

Quantification of in Vivo Tumor Burden. Rat and mouse livers were cut into 3-mm slices before embedding and sectioning. Limits of malignancy were defined on H&E sections from each block (five per liver) by a histopathologist blinded to the regime. Tumor area as a proportion of liver area was quantified with Image J (NIH).

Statistical Analyses. Analyses were performed with Prism (GraphPad v5). Data are presented as mean ± SEM. Data distribution was assessed using the D'Agostino & Pearson normality test and comparisons between two groups using the Student t test or Mann–Whitney U test; multiple groups were compared with the one-way ANOVA or Kruskal–Wallis test. Post hoc testing groups of nonparametric data were performed using Dunn's multiple comparison test.

ACKNOWLEDGMENTS. CK19CreER^{T}R26ReYFP mice were a gift from G. Gu (Vanderbilt University Medical Center). R.V.G. and T.J.K. are funded by Wellcome Trust fellowships. L.B., W.-Y.L., A.R., and S.J.F. are funded by the Medical Research Council, Cancer Research UK (CRUK), and the Alan Morement Memorial Fund (AMMF) charity. A.J.R. and S.E.M.-L. are funded by Medical Research Council fellowships. J.P.M. is funded by CRUK. O.J.S. is funded by the European Research Council and CRUK.

1. Zong Y, et al. (2009) Notch signaling controls liver development by regulating biliary differentiation. *Development* 136(10):1727–1739.
2. Boulter L, et al. (2012) Macrophage-derived Wnt opposes Notch signaling to specify hepatic progenitor cell fate in chronic liver disease. *Nat Med* 18(4):572–579.
3. Ortica S, Tarantino N, Aulner N, Israel A, Gupta-Rossi N (2014) The 4 Notch receptors play distinct and antagonistic roles in the proliferation and hepatocytic differentiation of liver progenitors. *FASEB J* 28(2):603–614.
4. Mazur PKEH, et al. (2010) Notch2 is required for progression of pancreatic intraepithelial neoplasia and development of pancreatic ductal adenocarcinoma. *Proc Natl Acad Sci USA* 107(30):13438–13443.
5. Font-Burgada J, et al. (2015) Hybrid periportal hepatocytes regenerate the injured liver without giving rise to cancer. *Cell* 162(4):766–779.
6. Fan B, et al. (2012) Cholangiocarcinomas can originate from hepatocytes in mice. *J Clin Invest* 122(8):2911–2915.
7. Zender S, et al. (2013) A critical role for notch signaling in the formation of cholangiocellular carcinomas. *Cancer Cell* 23(6):784–795.
8. Tarlow BD, et al. (2014) Bipotential adult liver progenitors are derived from chronically injured mature hepatocytes. *Cell Stem Cell* 15(5):605–618.
9. Yeh C-NMA, Maitra A, Lee KF, Jan YY, Chen MF (2004) Thioacetamide-induced intestinal-type cholangiocarcinoma in rat: An animal model recapitulating the multistage progression of human cholangiocarcinoma. *Carcinogenesis* 25(4):631–636.
10. Huppert SS, et al. (2000) Embryonic lethality in mice homozygous for a processing-deficient allele of Notch1. *Nature* 405(6789):966–970.
11. Krebs LT, et al. (2003) Characterization of Notch3-deficient mice: Normal embryonic development and absence of genetic interactions with a Notch1 mutation. *Genesis* 37(3):139–143.
12. Khan SATH, Thomas HC, Toledano MB, Cox IJ, Taylor-Robinson SD (2005) p53 Mutations in human cholangiocarcinoma: A review. *Liver Int* 25(4):704–716.
13. Guest RV, et al. (2014) Cell lineage tracing reveals a biliary origin of intrahepatic cholangiocarcinoma. *Cancer Res* 74(4):1005–1010.
14. Means ALXYX, Xu Y, Zhao A, Ray KC, Gu G (2008) A CK19(^{CreERT}) knockin mouse line allows for conditional DNA recombination in epithelial cells in multiple endodermal organs. *Genesis* 46(6):318–323.
15. Shimizu Y, et al. (1992) Two new human cholangiocarcinoma cell lines and their cytogenetics and responses to growth factors, hormones, cytokines or immunologic effector cells. *Int J Cancer* 52(2):252–260.
16. Villanueva A, et al. (2012) Notch signaling is activated in human hepatocellular carcinoma and induces tumor formation in mice. *Gastroenterology* 143(6):1660–1669.
17. Andersen JBSB, et al. (2012) Genomic and genetic characterization of cholangiocarcinoma identifies therapeutic targets for tyrosine kinase inhibitors. *Gastroenterology* 142(4):1021–1031.e15.
18. Huntzicker EG, et al. (2015) Differential effects of targeting Notch receptors in a mouse model of liver cancer. *Hepatology* 61(3):942–952.
19. Ahn S, Hyeon J, Park CK (2013) Notch1 and Notch4 are markers for poor prognosis of hepatocellular carcinoma. *Hepatobiliary Pancreat Dis Int* 12(3):286–294.
20. Bellavia D, et al. (2002) Combined expression of pTalpha and Notch3 in T cell leukemia identifies the requirement of preTCR for leukemogenesis. *Proc Natl Acad Sci USA* 99(6):3788–3793.
21. van Es JH, et al. (2005) Notch/gamma-secretase inhibition turns proliferative cells in intestinal crypts and adenomas into goblet cells. *Nature* 435(7044):959–963.
22. Ewald F, et al. (2013) Combined targeting of AKT and mTOR using MK-2206 and RAD001 is synergistic in the treatment of cholangiocarcinoma. *Int J Cancer* 133(9):2065–2076.
23. Ayaz F, Osborne BA (2014) Non-canonical notch signaling in cancer and immunity. *Front Oncol* 4:345.
24. Vacca A, et al. (2006) Notch3 and pre-TCR interaction unveils distinct NF-kappaB pathways in T-cell development and leukemia. *EMBO J* 25(5):1000–1008.
25. Lee KS, et al. (2013) Roles of PINK1, mTORC2, and mitochondria in preserving brain tumor-forming stem cells in a noncanonical Notch signaling pathway. *Genes Dev* 27(24):2642–2647.
26. Chen X, et al. (2010) Jagged1 expression regulated by Notch3 and Wnt/β-catenin signaling pathways in ovarian cancer. *Oncotarget* 1(3):210–218.
27. Lu WY, et al. (2015) Hepatic progenitor cells of biliary origin with liver repopulation capacity. *Nat Cell Biol* 17(8):971–983.